



# Demonstration of a highly subluminal laser with suppression of cavity length sensitivity by nearly three orders of magnitude

JOSHUA YABLON,<sup>1,\*</sup> ZIFAN ZHOU,<sup>1</sup> NICHOLAS CONDON,<sup>1,2</sup> DEVIN HILEMAN,<sup>1,2</sup> SHIH TSENG,<sup>1,2</sup> AND SELIM SHAHRIAR<sup>1,3</sup>

<sup>1</sup>Department of Electrical Engineering and Computer Science, Northwestern University, Evanston, IL, USA

<sup>2</sup>Digital Optics Technologies, Inc., Rolling Meadows, IL, USA

<sup>3</sup>Department of Physics and Astronomy, Northwestern University, Evanston, IL, USA

\*[yablon@u.northwestern.edu](mailto:yablon@u.northwestern.edu)

**Abstract:** We have demonstrated a laser in which the frequency shift due to small cavity fluctuations is far less than what would be expected from a conventional laser. The factor of sensitivity suppression is inferred to be equal to the effective group index experienced by the laser, implying that this laser is subluminal. We have observed a suppression factor as high as 663. Such a laser is highly self-stabilized compared to a conventional laser, and is expected to have a far smaller Schawlow-Townes linewidth. As a result, this laser may have potentially significant applications in the fields of high-precision optical metrology and passive frequency stabilization.

© 2017 Optical Society of America under the terms of the [OSA Open Access Publishing Agreement](#)

**OCIS codes:** (140.3550) Lasers, Raman; (260.2030) Dispersion.

## References and links

1. M. S. Shahriar, G. S. Pati, R. Tripathi, V. Gopal, M. Messall, and K. Salit, "Ultrahigh enhancement in absolute and relative rotation sensing using fast and slow light," *Phys. Rev. A* **75**, 053807 (2007).
2. H. N. Yum, M. Salit, J. Yablon, K. Salit, Y. Wang, and M. S. Shahriar, "Superluminal ring laser for hypersensitive sensing," *Opt. Express* **18**(17), 17658–17665 (2010).
3. G. S. Pati, M. Salit, K. Salit, and M. S. Shahriar, "Demonstration of displacement-measurement-sensitivity proportional to inverse group index of intra-cavity medium in a ring resonator," *Opt. Commun.* **281**, 4931–4935 (2008).
4. G. S. Pati, M. Salit, K. Salit, and M. S. Shahriar, "Simultaneous slow and fast light effects using probe gain and pump depletion via Raman gain in atomic vapor," *Opt. Express* **17**(11), 8775–8780 (2009).
5. D. D. Smith, K. Myneni, H. Chang, A. Toftul, C. Schambeau, J. A. Odutola, and J. C. Diels, "Tuning the sensitivity of an optical cavity with slow and fast light," *Proc. SPIE* **8273**, 82730T (2012).
6. N. B. Phillips, I. Novikova, E. E. Mikhailov, D. Budker, and S. Rochester, "Controllable steep dispersion with gain in a four-level N-scheme with four-wave mixing," *J. Mod. Opt.* **60**(1), 64–72 (2013).
7. M. Sabooni, Q. Li, L. Rippe, R. K. Mohan, and S. Kröll, "Spectral engineering of slow light, cavity line narrowing, and pulse compression," *Phys. Rev. Lett.* **111**(18), 183602 (2013).
8. Z. Zhou, J. Yablon, M. Zhou, Y. Wang, A. Heifetz, and M. S. Shahriar, "Modeling and analysis of an ultrastable subluminal laser," *Opt. Commun.* **358**, 6–19 (2016).
9. C. Henry, "Theory of the Linewidth of Semiconductor Lasers," *IEEE J. Quantum Electron.* **18**(2), 259–264 (1982).
10. M. A. Biot, "General theorems on the equivalence of group velocity and energy transport," *Phys. Rev.* **105**(4), 1129–1137 (1957).
11. M. O. Scully and W. E. Lamb, *Laser Physics* (Westview, 1974).
12. J. Yablon, Z. Zhou, M. Zhou, Y. Wang, S. Tseng, and M. S. Shahriar, "Theoretical modeling and experimental demonstration of Raman probe induced spectral dip for realizing a superluminal laser," *Opt. Express* **24**(24), 27444–27456 (2016).
13. H. C. Bolton and G. J. Troup, "The modification of the Kronig-Kramers relations under saturation conditions," *Philos. Mag.* **19**(159), 477–485 (1969).
14. G. J. Troup and A. Bambini, "The use of the modified Kramers-Kronig relation in the rate equation approach of laser theory," *Phys. Lett.* **45**(5), 393–394 (1973).
15. H. N. Yum and M. S. Shahriar, "Pump-probe model for the Kramers-Kronig relations in a laser," *J. Opt.* **12**(10), 104018 (2010).

16. Y. Wang, Z. Zhou, J. Yablon, and M. S. Shahriar, "Effect of multiorde harmonics in a double-Raman pumped gain medium for a superluminal laser," *Opt. Eng.* **54**(5), 057106 (2015).
17. "Vapor pressure of the metallic elements", in *CRC Handbook of Chemistry and Physics*, Internet Version 2005, David R. Lide, ed., <<http://www.hbcnetbase.com>>, CRC Press, Boca Raton, FL, 2005.
18. D. Phillips, "Notes on the Rb Maser and the CPT Clock," <https://www.cfa.harvard.edu/~dphil/work/rbmaser/masernotes.pdf>.
19. M. S. Shahriar, Y. Wang, S. Krishnamurthy, Y. Tu, G. S. Pati, and S. Tseng, "Evolution of an N-level system via automated vectorization of the Liouville equations and application to optically controlled polarization rotation," *J. Mod. Opt.* **61**(4), 351–367 (2014).

## 1. Introduction

Recent studies [1–8] have shown that the resonant frequency of a cavity is less sensitive to change in length when a slow light medium is placed inside the cavity. In a recent paper [8], we described the active version of such a cavity, a so-called subluminal laser (SLL). Briefly, an SLL is a laser in which  $v_g$ , the group velocity of the intra-cavity lasing beam, is significantly slower than the vacuum speed of light. The spectral sensitivity, defined as the shift in resonant frequency as a function of cavity length change, is reduced by a factor of  $n_g$ , the group index, which is defined as the ratio between the vacuum speed of light and  $v_g$ . Since very high values of  $n_g$  can be achieved experimentally, an SLL can be an ultra-stable laser. Another interesting and potentially very important aspect of the SLL is that its quantum noise limited linewidth (known as the Schawlow-Townes linewidth, or STL) is expected to be smaller than that of a conventional laser by a factor of  $n_g^2$ . This conclusion is based on the argument that the energy flow rate is proportional to  $v_g$  [9]. However, as shown in [10], this relationship is not valid when the dispersion is anomalous, so that this expected dependence of STL on  $n_g$  only applies when  $n_g \geq 1$ . In this paper, we report the demonstration of an SLL with tunable group index, reaching values of  $n_g$  as high as 663. Such an SLL may find important applications in precision metrology and laser stabilization.

## 2. Theory

The phase and amplitude of an electromagnetic wave inside a cavity are governed by the single-mode laser equations [11]:  $\partial\varphi/\partial t = (\Omega_c - \omega) - \omega\chi_r/2$  and  $\partial E/\partial t = -\omega E/2Q - \omega\chi_l E/2$ , where  $\omega$ ,  $\varphi$ , and  $E$  are the electric field frequency, phase, and amplitude, respectively,  $\Omega_c$  is the empty cavity resonance frequency,  $Q$  is the cavity quality factor, and  $\chi \equiv \chi_r + i\chi_l$  is the effective susceptibility experienced by the lasing beam. If the roundtrip length of the cavity is changed by a differential amount  $dL$ , the resulting frequency shift is  $(\partial f/\partial L) \cdot dL \equiv S_L \cdot dL$ , where  $S_L$  is the spectral sensitivity of the laser. The spectral sensitivity of the empty cavity resonance is  $S_{EC} \equiv \partial\Omega_c/\partial L$  so that the ratio  $S_{EC}/S_L$  is the Sensitivity Suppression Factor (SSF). Solving the single-mode laser equations in steady state [12] results in:  $SSF = 1 + \chi_r/2 + (\omega/2)(\partial\chi_r/\partial\omega) \approx n_g$ . This expression is valid as long as  $|\chi_r| \ll 1$ , which is the case for dilute atomic vapor. The Kramers-Kronig relations [13–15] imply that positive dispersion generally occurs in a transmission (or gain) peak, while negative dispersion generally occurs in a transmission (or gain) dip. Therefore, if the goal is to create a highly subluminal laser, a logical approach would be finding a gain mechanism with a very narrow gain bandwidth. A laser making use of Raman gain in atomic alkali vapor is an excellent candidate, because two-photon resonant processes in alkali atoms are very narrow, with linewidths generally on the order of ~1 MHz [4].

One of the constraints in using Raman gain to make an SLL is that the linewidth of the gain, which must be narrow for producing a substantial SSF, tends to increase with increasing value of peak gain. This dependence can be understood by noting that the effective population inversion between the two metastable states, needed for Raman gain, is produced via optically pumping atoms from one of these states to the other. This rate of optical pumping serves as an effective decay rate, which, along with collisional dephasing rate of the coherence between

the two metastable states, determines the width of the Raman gain. In order to circumvent this constraint, we, in Ref. 8, proposed a design for an SLL where Raman gain produced in an alkali vapor cell is combined with the so-called DPAL (Diode-Pumped Alkali Laser) gain, which can be very strong and broad, and is produced in an alkali vapor cell loaded with buffer gas. In such a system, a high output power laser can be produced while still achieving a significant SSF. Aside from the obvious utility of high output power, it should also be noted that the STL decreases with increasing power. Thus, such a hybrid system should still be the preferred method for making an SLL. The work demonstrated here is meant to establish the degree of SSF that can be achieved using the Raman gain by itself.

### 3. Experiment

The subluminal laser makes use of Raman gain in  $^{85}\text{Rb}$  vapor inside a ring resonator. The relevant energy levels, as shown in Fig. 1(a), are denoted as follows:  $|1\rangle \equiv S_{1/2}(F=2)$ ;  $|2\rangle \equiv S_{1/2}(F=3)$ ;  $|3\rangle \equiv P_{1/2}$  manifold;  $|4\rangle \equiv P_{3/2}$  manifold. An optical pumping beam couples  $|2\rangle$  to  $|4\rangle$  in order to transfer atoms from  $|2\rangle$  to  $|1\rangle$ . This results in an effective decay rate from  $|2\rangle$  to  $|1\rangle$ , as indicated in Fig. 1(b), and therefore creates Raman population inversion between these two states. The Raman pump is applied on the  $|1\rangle \rightarrow |3\rangle$  transition with a detuning,  $\Delta_{\text{RP}}$ , on the order of 1 GHz. The presence of these beams produces a Raman gain on the  $|2\rangle \rightarrow |3\rangle$  transition. If a probe is applied on this transition with a detuning of  $\Delta_{\text{L}}$ , then the gain is maximized under the condition of two-photon resonance:  $\delta \equiv \Delta_{\text{L}} - \Delta_{\text{RP}} = 0$ . Under typical operating conditions, the width of the Raman gain is  $\sim 1$  MHz. The Raman pump is s-polarized, which produces gain for a probe that is p-polarized, due to the signs of the relevant matrix elements that couple the Zeeman sublevels along the  $|1\rangle \rightarrow |3\rangle$  and  $|2\rangle \rightarrow |3\rangle$  transitions. At experimental temperatures ( $\sim 100^\circ\text{C}$ ), the optical transitions are Doppler-broadened with a FWHM of  $\sim 560$  MHz. Since the Raman gain spectrum is much narrower than this, the probe gain is far higher when it is co-propagating with the Raman pump than when it is counter-propagating [16]. As a result, the subluminal laser always operates in the same direction as the Raman pump.

In Fig. 1, the Raman pump and the optical pump are on the  $S_{1/2}(F=2) \rightarrow P_{1/2}$  and  $S_{1/2}(F=3) \rightarrow P_{3/2}$  transitions, respectively, resulting in lasing on the  $S_{1/2}(F=3) \rightarrow P_{1/2}$  transition. In what follows, this will be referred to as “configuration A.” However, a subluminal laser can just as easily be realized by placing the Raman pump and the optical pump on the  $S_{1/2}(F=3) \rightarrow P_{1/2}$  and  $S_{1/2}(F=2) \rightarrow P_{3/2}$  transitions, respectively, resulting in lasing on the  $S_{1/2}(F=2) \rightarrow P_{1/2}$  transition; this will be referred to as “configuration B”. It is also important to note that there are two hyperfine levels in the  $P_{1/2}$  manifold ( $F=2$  and  $F=3$ , which are split by approximately 362 MHz). For both configurations,  $\Delta_{\text{RP}}$  is defined as the Raman pump detuning relative to the midpoint between these two hyperfine levels.

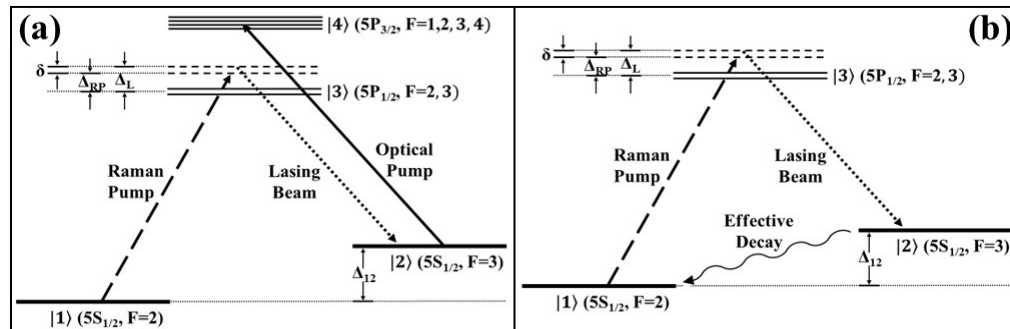


Fig. 1. (a) Energy levels and optical fields involved in the subluminal laser (configuration A); (b) Energy levels and optical fields corresponding to (a), but with the optical pump modeled as an effective decay rate.

The experimental setup is illustrated schematically in Fig. 2(a). The Raman pump, generated from a Toptica DL-Pro 100 external cavity diode laser with a typical linewidth of 10 kHz and tuned to  $^{85}\text{Rb}$  D<sub>1</sub> line (794.767 nm), is s-polarized and inserted into the lasing cavity using a polarizing beam splitter (PBS). It is then expelled from the cavity using another PBS, after passing through a vapor cell containing isotopically pure  $^{85}\text{Rb}$  atoms. The optical pumping beam, generated from a Photodigm DBR diode laser with a typical linewidth of 0.7 MHz and tuned to  $^{85}\text{Rb}$  D<sub>2</sub> line (780.036 nm), is also s-polarized, and is inserted into and expelled from the cavity using the same pair of PBS's, but in the opposite direction. The cavity is a square with a perimeter of 1 meter. A lens with focal length of 750 cm is used to stabilize the cavity. The minimum waist size of the lasing mode occurs exactly opposite the location of the lens; an iris is placed at that location to spatially filter out all transverse modes besides the TEM<sub>00</sub> mode. A beam splitter (BS) diverts a small fraction of the Raman pump, which is combined with the Raman laser output and sent into a photodetector (PD); the resulting beat note has a frequency of  $f_B = f_{RP} - f_L = \Delta_{12} - \delta$  where  $\Delta_{12}$ , the hyperfine splitting between the  $F = 2$  and  $F = 3$  ground states in  $^{85}\text{Rb}$  (states  $|1\rangle$  and  $|2\rangle$ ), is approximately 3.0357 GHz. In order to scan the cavity length, one of the cavity mirrors is attached to a piezo-electric transducer (PZT). The Raman pump frequency remains fixed while the mirror position is scanned, which causes the beat frequency to change accordingly. The PD, with a bandwidth of 12.5 GHz and responsivity of 0.53 A/W, converts this beat note into an electrical signal, which is heterodyned with a stable reference signal with a frequency 3.2 MHz less than  $\Delta_{12}$ . The output of the heterodyning process therefore has a frequency centered around 3.2 MHz, which is then demodulated to produce a DC voltage proportional to the frequency. Having a 3.2 MHz central frequency enables us to distinguish between positive and negative values of  $\delta$ , provided that  $\delta$  remains above  $-3.2$  MHz ( $|\delta|$  is less than the Raman gain width, which is  $\sim 1$  MHz, as noted earlier). Two examples of plots showing input voltage (proportional to length change) versus output voltage (proportional to frequency shift) are shown in Figs. 2(b) and 2(c). Such plots are used to determine the laser frequency sensitivity to length change, which is compared with the sensitivity of an empty cavity to determine the SSF.

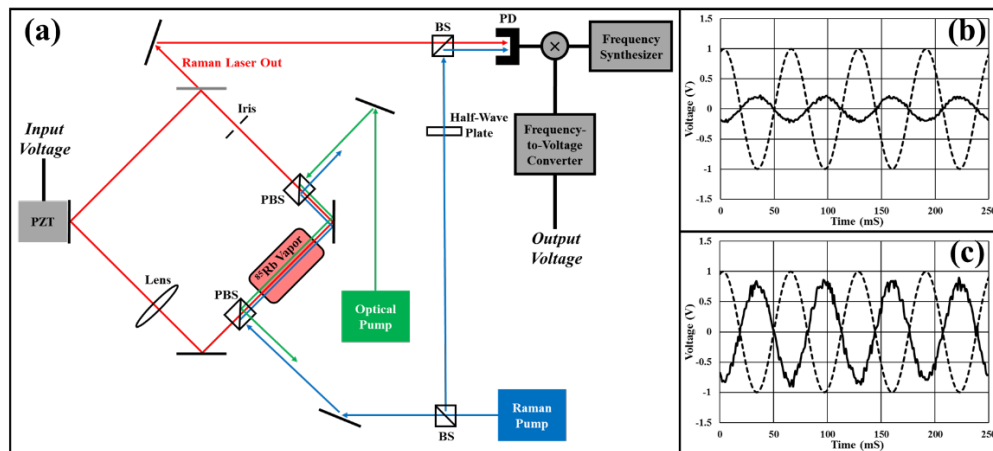


Fig. 2. (a) Schematic of the Raman laser and measurement system used to determine the SSF; (b) One example of an oscilloscope measurement produced by this experiment. The dotted line is the PZT input voltage, while the solid line is the demodulator output voltage; (c) Another example of an oscilloscope measurement. Though the peak-to-peak input voltage is the same as in (b), the peak-to-peak output voltage is larger than in (b), implying a lower SSF.

There are several experimental parameters which can affect the output power and the SSF of the subluminal laser. Accordingly, these values were measured for many combinations of

vapor temperature, Raman pump power, optical pump power, output coupler reflectivity, Raman pump detuning, and configuration. Figure 3 illustrates how the temperature and the Raman pump detuning affect the SSF. All the data in Fig. 3 were taken with the optical fields in configuration B, 2.5 mW Raman pump power, 58 mW optical pump power, and 80% output coupler reflectivity. At a given cell temperature, the SSF evidently increases as resonance is approached; however, when too close to resonance, lasing cannot occur due to increased absorption resulting from the proximity to the optical transition. The inset figure shows the SSF versus temperature at  $\Delta_{RP} = 1800$  MHz and  $\Delta_{RP} = 2100$  MHz. The SSF increases as temperature increases from 100°C to 115°C, but then decreases from 115°C to 130°C and then to 145°C. The SSF is therefore maximized at some temperature,  $T_{MAX}$ , which in this case is somewhere between 100°C and 130°C. In general,  $T_{MAX}$  can depend on many factors such as Raman pump intensity, optical pump intensity, output coupler reflectivity, and configuration. In order to interpret this behavior qualitatively, we note first that the vapor pressure has the following empirical relationship with temperature [17,18]:  $\log_{10}(P) = A + BT^{-1}$  where  $P$  is in atmospheres,  $T$  is in Kelvin,  $A = 4.312$  and  $B = -4040$ . For dilute atomic vapor, the number density  $n/V$  is related to pressure via the ideal gas law,  $n/V = P/k_B T$ . The number density therefore doubles approximately every 10-12°C in the experimental temperature range. In general, susceptibility increases with increasing atomic density. However, if the density reaches too high a value, the Raman pump and the optical pump become mostly or completely absorbed. This causes a decrease in the total overlap between the lasing mode and the Raman and optical pumps, thus reducing the effective susceptibility experienced by the laser. More detailed modeling, augmented by additional experimental data, would be needed to characterize the temperature dependence of the SSF in a quantitative manner.

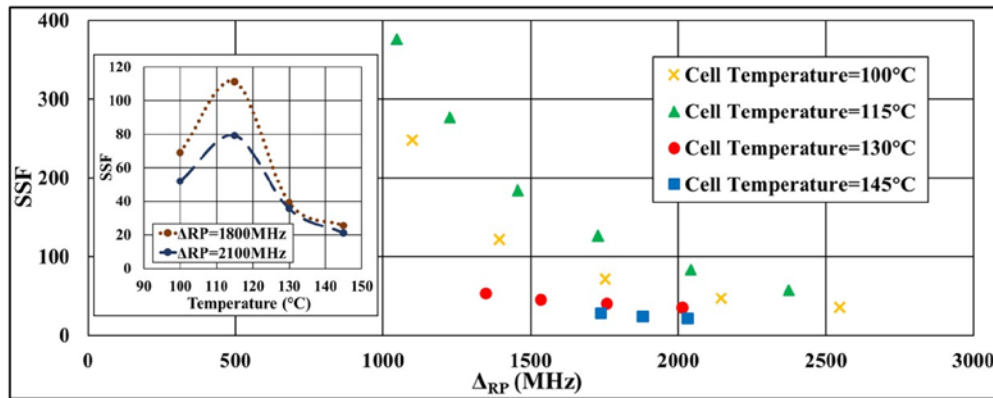


Fig. 3. Measured values of SSF versus  $\Delta_{RP}$  at four different temperatures. These data were then used to create the inset plots of SSF versus temperature at  $\Delta_{RP} = 1800$  and  $\Delta_{RP} = 2100$  MHz.

Figure 4 shows one example of how the SSF and the output power are affected by the power of the Raman pump. The data in Fig. 4 were taken with the energy levels in configuration A, 115°C cell temperature, 58 mW optical pump power, and 80% output coupler reflectivity. For this set of data, the Raman pump detuning is negative. Consider first the behavior of the output power. With stronger Raman pump power, the output power is significantly higher, and lasing occurs over a wider range of  $\Delta_{RP}$ , as expected. It is also evident that in this case there is an optimal pump detuning that produces maximum output power. This is due to the fact that Raman gain increases as the Raman pump approaches resonance, but so does Doppler-broadened absorption of the Raman pump and the lasing beam. These two competing effects determine the detuning at which maximum lasing power is achieved. Consider next the behavior of the SSF. For a given value of  $\Delta_{RP}$ , the value of the

SSF is approximately 4 to 6 times higher for the weaker Raman pump. This behavior can be understood qualitatively by noting that the width of the Raman gain is power broadened for a strong Raman pump, thus decreasing the slope of the dispersion.

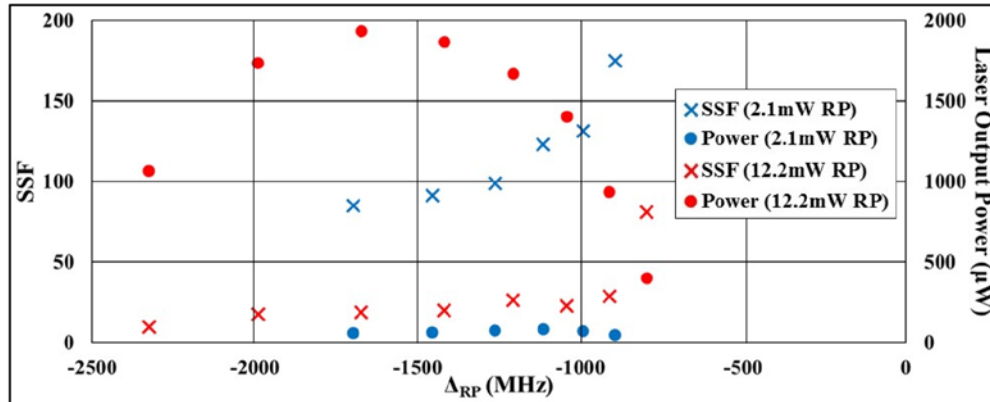


Fig. 4. SSF (left axis) and output power (right axis) vs. detuning, using two different values of Raman pump power

Figure 5 compares data obtained with a 50% reflectivity output coupler (OC) to that obtained with an 80% reflectivity OC. The data in Fig. 5 were taken with the energy levels in configuration A, 115°C cell temperature, 200 mW optical pump power, and 2.1 mW Raman pump power. For all values of Raman pump detuning, the OC reflectivity does not appear to make a significant difference in the SSF. However, the OC with the lower reflectivity enables operation of the laser at a value of  $|\Delta_{RP}|$  that is closer to resonance. Since SSF increases as the Raman pump approaches resonance, the highest achievable SSF with the 50% OC was greater than that with the 80% OC.

It should be noted that the cavity finesse for a 50% OC is much lower than that for an 80% OC. Thus, a much stronger optical pumping beam was necessary to produce stable Raman lasing for 50% OC. For the data shown in Fig. 5, we used the high level of optical pumping power for both cases (50% OC and 80% OC) in order to make the comparison between these two cases more meaningful.

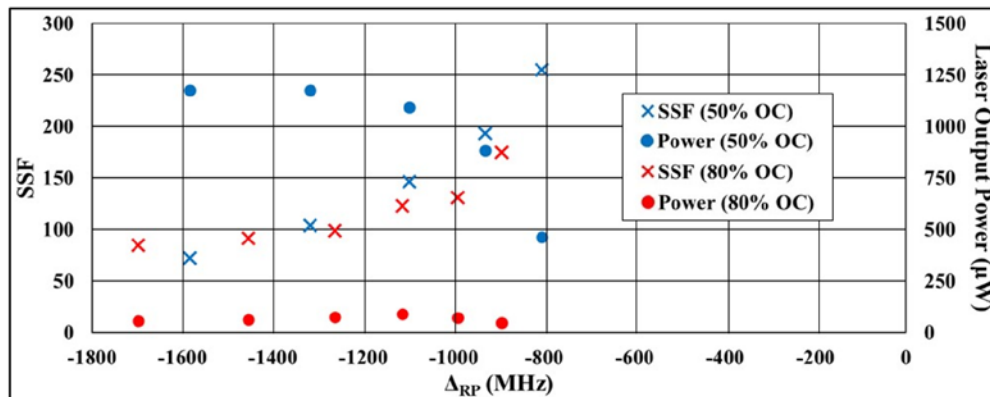


Fig. 5. SSF (left axis) and output power (right axis) vs. detuning, using two different output coupler reflectivities

The highest SSF achieved during the experiment (with a value of 663) is presented in Fig. 6, which also shows that the SSF is not symmetric with respect to the sign of  $\Delta_{RP}$ . All the data in Fig. 6 were taken with the energy levels in configuration A, 200 mW optical pump power,

2.1 mW Raman pump power, and a 50% OC. We generally see larger values of SSF for positive  $\Delta_{RP}$  than for negative  $\Delta_{RP}$ , despite the fact that the laser is able to operate closer to resonance for negative  $\Delta_{RP}$ . Additionally,  $T_{MAX}$  appears to depend on the sign of  $\Delta_{RP}$ ; 85°C yielded the lowest values of SSF for negative  $\Delta_{RP}$ , but yielded the highest values for positive  $\Delta_{RP}$ . These asymmetries are possibly due to the fact that states  $|1\rangle$ ,  $|2\rangle$ , and  $|3\rangle$  contain five, seven, and twelve Zeeman sub-levels, respectively. Each sub-level has its own unique matrix element and therefore contributes differently to the two-photon gain and lasing processes for different signs of  $\Delta_{RP}$ .

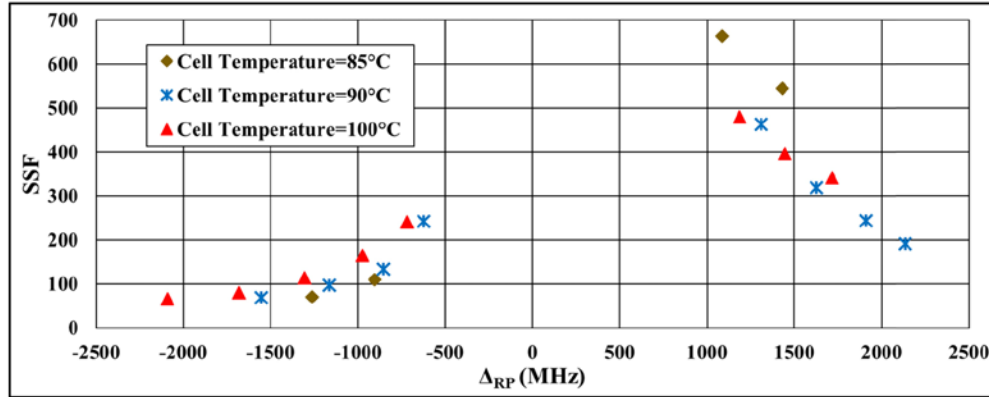


Fig. 6. SSF vs. detuning, for positive and negative values of  $\Delta_{RP}$ , at three different temperatures

One ubiquitous effect is that for all combinations of experimental parameters, the SSF increases as the Raman pump approaches resonance. There are two factors which possibly cause this universal trend: the positive dispersion profile outside of a Doppler-broadened resonance, and narrowing of two-photon laser gain as  $\Delta_{RP}$  and  $\Delta_L$  approach zero. It is not clear as to how much each effect contributes to the effective dispersion of the lasing beam; however, the simulations, described in the next section, agree with this trend.

There were two more parameters considered during this experiment: optical pump power and configuration. While the optical pump power affects the output power of the laser, it does not appear to affect the SSF drastically. Meanwhile, configuration does not appear to make a significant difference in the output power nor the SSF.

As previously mentioned, the STL of a subluminal laser is predicted [9] to be reduced by a factor of  $n_g^2$  relative to a conventional laser. The standard formula for the full-width half maximum (FWHM) STL, without considering the effect of dispersion, is:  $\Delta f_{ST} = hf_o / (4\pi P_{OUT} \tau_c^2)$ , where  $f_o$  is the laser frequency,  $\tau_c$  is the empty cavity decay time, given by  $R^{1/4}L / [(1 - R^{1/2})c]$ , where  $R$  is the intensity reflectivity of the output coupler, and  $P_{OUT}$  is the laser output power. For a laser with  $R = 0.5$  and  $P_{OUT} = 400 \mu\text{W}$ , the value of  $\Delta f_{ST}$  is  $\sim 560$  mHz. For  $n_g = 663$ , assuming a suppression factor of  $n_g^2$ , the value of  $\Delta f_{ST}$  would be  $\sim 1.2 \mu\text{Hz}$ . Of course, it should be noted that many sources of non-idealities in the experiment may keep  $\Delta f_{ST}$  from reaching such a low value. Nonetheless, it would be important to investigate experimentally whether  $\Delta f_{ST}$  for a subluminal laser is indeed substantially lower than what would be expected without the effect of dispersion. However, our current system is not stabilized enough to carry out this investigation. We are currently working on implementing advanced techniques that may enable us to reach a degree of stability high enough to measure very small values of  $\Delta f_{ST}$ , directly or indirectly.

#### 4. Simulation

Because of the numerous variables and interconnected processes occurring in the subluminal laser (AC Stark shifts, Doppler broadening, spectral hole burning, etc.), numerical methods are necessary to provide a quantitative model of the laser behavior. Our simulation solves the single-mode laser equations (as summarized in section 2) and the density matrix equations in an iterative fashion until a steady-state solution is reached [8,19].

In the single-mode laser equations,  $\chi$  is the effective susceptibility experienced by the lasing beam during one round trip. The gain cell in the experiment was 8 cm long while the cavity perimeter was 60 cm, so that only  $\sim 13\%$  of the cavity was filled with gain. Because  $\chi$  depends on the total number of atoms interacting with the lasing beam in one round trip, the calculation assumes that the gain medium fills the entire cavity with a number density equal to  $\sim 13\%$  of the gain cell number density. This also means that the group index experienced by the lasing beam *inside the vapor cell* is  $\sim 7.5$  times the SSF. For example, when the SSF of the subluminal laser was measured to be 663, the group index of the gain cell was almost 5,000.

The Liouville equation, describing the evolution of the gain medium, is  $\partial \tilde{\rho} / \partial t = -i/\hbar [\tilde{H}, \tilde{\rho}] + \partial \tilde{\rho}_{SOURCE} / \partial t$ , where  $\tilde{\rho}$  and  $\tilde{H}$  are the density matrix of the atoms, and the modified Hamiltonian that includes the effect of population decays, respectively, in the rotating wave basis. The source term accounts for the influx of atoms into the relevant atomic states. Figure 7(a) shows how the three-level system is modeled in configuration B. The optical pump is treated as a decay rate from  $|1\rangle$  to  $|2\rangle$ , denoted as  $\Gamma_{OP}$ . The lasing beam couples states  $|1\rangle$  and  $|3\rangle$  while the Raman pump couples states  $|2\rangle$  and  $|3\rangle$  with coupling strengths (i.e. Rabi frequencies) of  $\Omega_L$  and  $\Omega_{RP}$ , respectively. The natural decay rate from state  $|i\rangle$  to  $|j\rangle$  is denoted as  $\Gamma_{ij}$  ( $i, j = 1, 2, 3$ ).  $\chi$  is governed by the following relationship:  $\chi = \tilde{\rho}_{31} (\hbar c n / I_{SAT(13)} \Omega_L) (\Gamma_{31} / 2)^2$ , where  $n$  is atomic number density and  $I_{SAT(13)}$  is the effective saturation intensity of the  $|1\rangle \rightarrow |3\rangle$  transition, which is approximately  $8.35 \text{ mW/cm}^2$  [12]. The algorithm then solves the single-mode laser equations and Liouville equation in an iterative fashion until a steady-state solution is reached. To compute the SSF, this calculation must be performed for two different cavity roundtrip lengths:  $L_o$  and  $L_o + dL$ , where  $L_o$  is the initial cavity length and  $dL$  is a small perturbation in length. The sensitivity of this laser,  $df/dL$ , is compared to that of an empty cavity to determine the SSF. Figure 7(b) shows two examples of the simulation output.

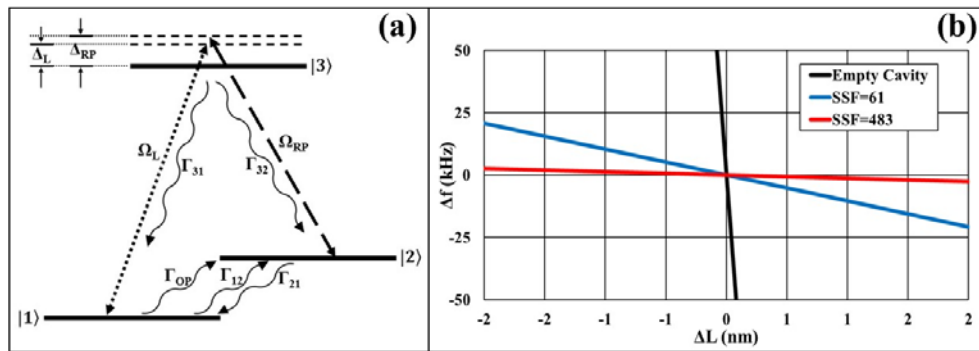


Fig. 7. (a) Energy levels, coupling fields, and decay rates used in the simulation, corresponding to configuration B; (b) The SSF is the ratio between the “empty cavity” slope ( $df_{ec}/dL$ ) and the laser output slope ( $df/dL$ ).

Figure 8 compares simulation results with experimental results for the following set of parameters: 2.5 mW Raman pump power, 58 mW optical pump power, 80% output coupler reflectivity,  $115^\circ\text{C}$  cell temperature, configuration B. There appears to be good qualitative match, showing increasing SSF as resonance is approached. There are several potential

reasons why simulation results do not match up more accurately with experimental results. First, we use a three-level model, where the optical pump is treated as a decay rate. In reality, states  $|1\rangle$  and  $|2\rangle$  contain 5 and 7 Zeeman sublevels, respectively; state  $|3\rangle$  contains two hyperfine levels, which contain 12 Zeeman sublevels in total; state  $|4\rangle$  contains four hyperfine levels, which contain 24 Zeeman sublevels in total. Therefore, the experimental process corresponds to a 48-level system. The matrix used in the algorithm [8,12,19] has dimensions of  $N^2 \times N^2$  (where  $N$  is the number of energy levels), so that a 48-level system is  $(48/3)^4 = 65536$  times as data-intensive as a three-level system, which takes typically 30 seconds to solve. Another limitation is the assumption that each optical field couples only two energy levels. For example, the Raman pump [Fig. 7(a)] is assumed to couple states  $|2\rangle$  and  $|3\rangle$ , but not states  $|1\rangle$  and  $|3\rangle$ . This is not entirely true, but the Rotating-Wave Approximation relies on this assumption. In principle, this constraint can be circumvented by using the Floquet technique where the solution is made up of a truncated set of harmonics [16]; however, for the iterative algorithm employed here, this process would be prohibitively time-consuming.

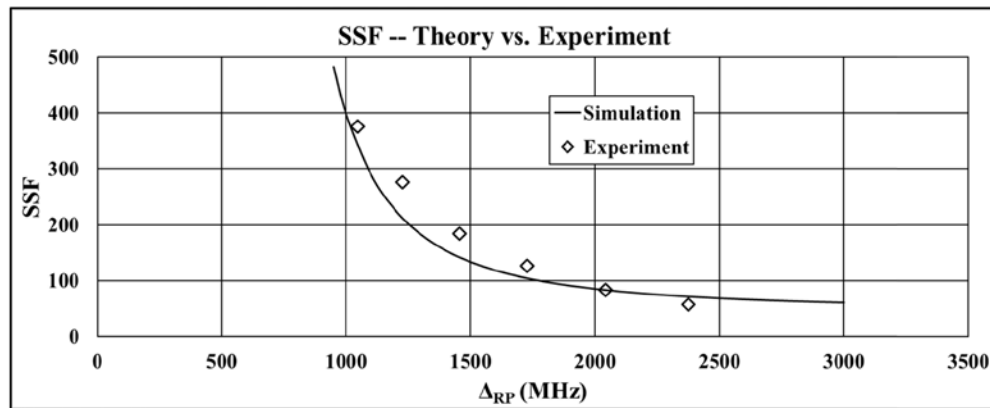


Fig. 8. SSF versus  $\Delta_{RP}$ : Comparison between simulation and experiment

## 5. Conclusion

We have demonstrated a laser with narrowband two-photon gain in which the frequency sensitivity is highly suppressed relative to a conventional laser. The factor of sensitivity suppression is inferred to be equal to  $n_g$ , the effective group index seen by the lasing beam. This increase in frequency stability by a factor of  $n_g$ , coupled with a linewidth which is expected to be inversely proportional to  $n_g^2$ , makes this laser promising for applications in precision metrology.

## Funding

DARPA (W911NF-15-1-0643); NASA (NNX16CM03C).